

Ascertaining *p,p'*-Dimercaptoazobenzene Produced from *p*-Aminothiophenol by Selective Catalytic Coupling Reaction on Silver NanoparticlesYurui Fang,[†] Yuanzuo Li,[†] Hongxing Xu,^{†,‡} and Mengtao Sun^{*†}[†]Beijing National Laboratory for Condensed Matter Physics, Institute of Physics, Chinese Academy of Sciences, P. O. Box 603-146, Beijing, 100190, People's Republic of China, and [‡]Division of Solid State Physics, Lund University, Lund 22100, Sweden

Received November 26, 2009. Revised Manuscript Received April 25, 2010

Combining experiment and theory, evidence from surface-enhanced Raman scattering (SERS) were obtained for *p,p'*-dimercaptoazobenzene (DMAB) produced from *p*-aminothiophenol (PATP) by selective catalytic coupling reaction on silver nanoparticles. The time-dependent SERS spectra of PATP are consistent with the calculated SERS spectra of DMAB, which is the direct evidence for the production of DMAB from PATP by selective catalytic coupling reaction on silver nanoparticles. The so-called “*b*₂ modes” of PATP is the –N=N– related vibrational modes of DMAB. The silver nanoparticles could be assembled together to form different size of aggregates with different concentration of PATP solution. When the concentration of Ag nanoparticle (the radius 40 nm) in colloid is 35 pM, the time-dependent SERS of DMAB reveals that the better experimental conditions for observing SERS signals of DMAB are (1) concentration of PATP is around 5×10^{-6} M in which condition the aggregates consist with about 3–5 silver nanoparticles, which are not too big and suitable for SERS measurement, and (2) the Raman signal will be strongest at the time delay about 27 min for this concentration. By analyzing the symmetry of strong enhanced vibrational modes, it is derived that all of six strong vibrational modes are mostly enhanced by surface plasmons (electromagnetic field). The SERS enhancement calculated with finite-difference time-domain method is on the order of $|M|^4 = 9.0 \times 10^8$ in junctions of AgNPs at 632.8 nm, where $|M| = E_{\text{loc}}/E_{\text{in}}$, and E_{loc} and E_{in} are local and incident electric fields, respectively. The total chemical enhancements, including static chemical and resonant enhancements, are on the order of 10^3 .

I. Introduction

Surface-enhanced Raman scattering (SERS) is widely used in chemistry, biology, physics, and material science, since it can enhance the inherently low Raman scattering cross sections of molecules, even at the level of single molecules.^{1–6} The electromagnetic (EM) and the chemical enhancement (CE) mechanisms are the two widely accepted mechanisms. The EM is caused by local surface plasmon polaritons,^{4,6} which usually enhances the Raman spectrum in a large frequency range. The CE results from the change of the electronic structures of molecule adsorbed on metal surfaces, where select Raman peaks are selectively enormously enhanced.^{7–11} Typically, the chemical enhancement is explained via the charge-transfer (CT) mechanism.

SERS of 4-aminothiophenol (PATP, see Figure 1a) adsorbed on different metal surfaces has been extensively studied

experimentally.^{12–23} Recently, there have been an increasing amount of attention paid to the study of the properties of metal–molecule–metal sandwich architectures,^{14,18–20,23} typically PATP interconnected by silver and gold nanoparticles. Strong *a*₁ and *b*₂ modes dominate the SERS spectra in the cases where molecules are attached to metal complexes and when molecules chemically locate in the junction of the metal–molecule–metal structure. These selective enhancements of *b*₂ modes were ascribed to the effect of chemical enhancement.

Recently, Wu and co-workers theoretically predicted that *p,p'*-dimercaptoazobenzene (DMAB, see Figure 1b) can be produced from PATP by catalytic coupling reaction on silver nanoparticles.²⁴ Theoretically, mechano and combined opto-mechano switching cycle of a single DMAB (also called 4,4'-dithioazobenzene)

*To whom correspondence should be addressed. E-mail: (M.T.S.) mtsun@aphy.iphy.ac.cn.

- (1) Fleischmann, M.; Hendra, P. J.; McQuillan, A. J. *Chem. Phys. Lett.* **1974**, *26*, 163.
- (2) Jeanmaire, D. L.; Van Duyne, R. P. *J. Electroanal. Chem.* **1977**, *84*, 1.
- (3) Albrecht, M. G.; Creighton, J. A. *J. Am. Chem. Soc.* **1977**, *99*, 5215.
- (4) Moskovits, M. *Rev. Mod. Phys.* **1985**, *57*, 783.
- (5) Kneipp, K.; Kneipp, H.; Itzkan, I.; Dasari, R. R.; Feld, M. S. *Chem. Rev.* **1999**, *99*, 2957.
- (6) Xu, H. X.; Bjerneld, E. J.; Kail, M.; Borjesson, L. *Phys. Rev. Lett.* **1999**, *83*, 4357.
- (7) Otto, A.; Mrozek, I.; Grabhorn, H.; Akemann, W. *J. Phys.: Condens. Mater.* **1992**, *4*, 1143.
- (8) Lombardi, J. R.; Birke, R. L. *J. Phys. Chem. C* **2008**, *112*, 5605.
- (9) Lombardi, J. R.; Birke, R. L.; Lu, T.; Xu, J. *J. Chem. Phys.* **1986**, *84*, 4174.
- (10) Zhao, L. L.; Jensen, L.; Schatz, G. C. *J. Am. Chem. Soc.* **2006**, *128*, 2911.
- (11) Sun, M. T.; Liu, S. S.; Chen, M. D.; Xu, H. X. *J. Raman Spectrosc.* **2009**, *40*, 137.
- (12) Hill, W.; Wehling, B. *J. Phys. Chem.* **1993**, *97*, 9451.

- (13) Osawa, M.; Matsuda, N.; Yoshii, K.; Uchida, I. *J. Phys. Chem.* **1994**, *98*, 12702.
- (14) Wang, J.; Zhu, T.; Fan, Z. F. *Acta Phys. Chem.* **1998**, *94*, 485.
- (15) Cao, L.; Diao, P.; Tong, L.; Zhu, T.; Liu, Z. F. *ChemPhysChem* **2005**, *6*, 913.
- (16) Gibson, J. W.; Johnson, B. R. *J. Chem. Phys.* **2006**, *124*, 064701.
- (17) Fromm, D. P.; Sundaramurthy, A.; Kinkhabwala, A.; Schuck, P. J.; Kino, G. S.; Moerner, W. E. *J. Chem. Phys.* **2006**, *124*, 061101.
- (18) Baia, M.; Toderas, F.; Baia, L.; Popp, J.; Astilean, S. *Chem. Phys. Lett.* **2006**, *422*, 127.
- (19) Zhou, Q.; Li, X. W.; Fan, Q.; Zhang, X. X.; Zheng, J. W. *Angew. Chem., Int. Ed.* **2006**, *45*, 3970.
- (20) Zhou, Q.; Zhao, G.; Chao, Y. W.; Li, Y.; Wu, Y.; Zheng, J. W. *J. Phys. Chem. C* **2007**, *111*, 1951.
- (21) Toderas, F.; Baia, M.; Baia, L.; Astilean, S. *Nanotechnology* **2007**, *18*, 255702.
- (22) Wang, Y. L.; Zou, X. Q.; Ren, W.; Wang, W. D.; Wang, E. K. *J. Phys. Chem. C* **2007**, *111*, 3259.
- (23) Zhou, Q.; Chao, Y. W.; Li, Y.; Wu, W.; Wu, Y.; Zheng, J. W. *ChemPhysChem* **2007**, *8*, 921.
- (24) Wu, D. Y.; Liu, X. M.; Huang, Y. F.; Ren, B.; Xu, X.; Tian, Z. Q. *J. Phys. Chem. C* **2009**, *113*, 18212.

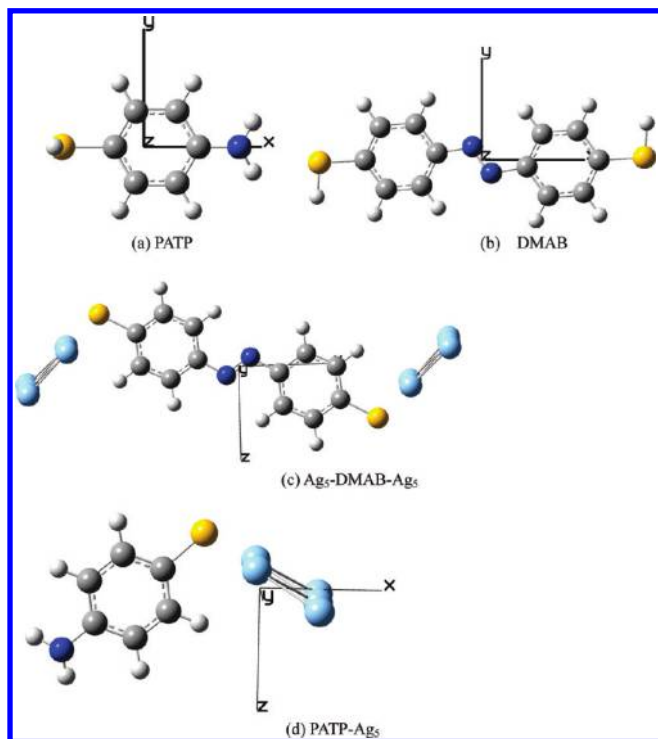


Figure 1. The chemical structures of (a) PATP, (b) DMAB, (c) Ag₅-DMAB-Ag₅ junction, and (d) PATP-Ag₅ complex, where the Cartesian coordinates were shown.

chromophore suspended between two gold tips have been investigated.²⁵ In previous studies, the so-called “b₂ modes” (Raman peaks at 1140, 1390, and 1432 cm⁻¹) can be clearly observed on silver nanoparticles,¹³ while the time-dependent SERS of PATP adsorbed on gold nanoparticles revealed that these three peaks are difficult to observe experimentally.²⁶ This means that DMAB can easily be produced from PATP through a catalytic coupling reaction on silver nanoparticles,^{13,24} but DMAB is difficult to produce by this catalytic coupling reaction on gold nanoparticles. Thus, it is very important to clarify the mechanisms by which and time scales over which these so-called “b₂ modes” occur, using time-dependent SERS both experimentally and theoretically.

In this paper, we provide the experimental and theoretical SERS evidence that DMAB can be produced from PATP by selective catalytic coupling reactions on silver nanoparticles. The time-dependent SERS spectra and theoretical analysis reveal the so-called “b₂ modes” of PATP are the -N=N- related vibrational modes of DMAB. Experimentally, when the concentration of Ag nanoparticle (the radius 40 nm) in colloid is 35 pM, the ideal concentration of PATP is 5×10^{-6} M under which condition the acquisition time of the strongest SERS of DMAB is at the twenty-seventh minute. We studied SERS electromagnetic and chemical mechanisms of DMAB. By analyzing the symmetry of strongly enhanced vibrational modes, we found that all six strong vibrational modes are primarily enhanced by plasmon (electromagnetic field). The electromagnetic field and chemical enhancements at the junctions of AgNPs at 632.8 nm were obtained through the finite-difference time-domain method and the quantum chemical method, respectively.

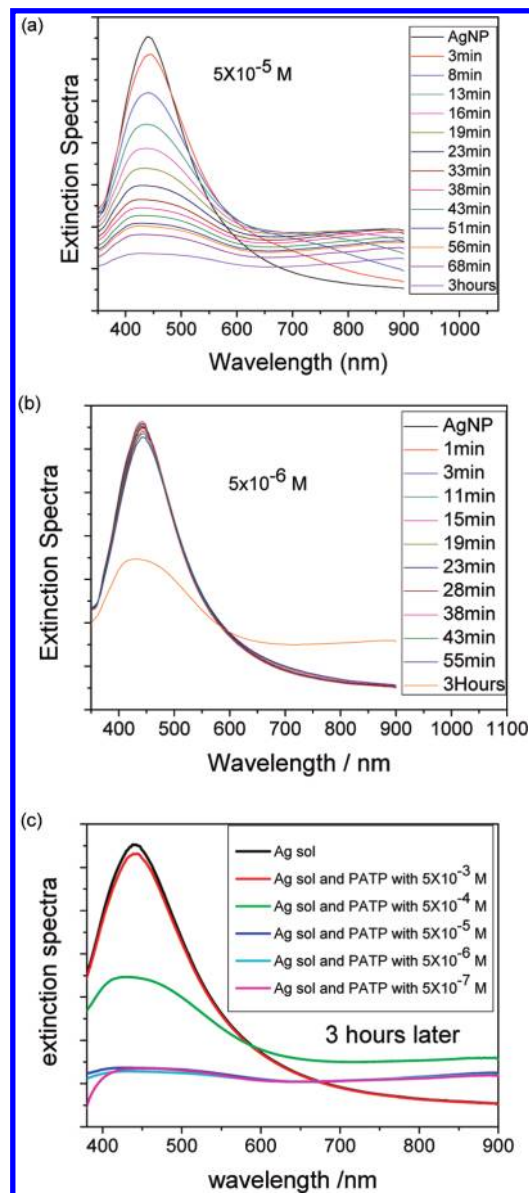


Figure 2. (a–c) Time-dependent extinction spectra of Ag sol and PATP in Ag sol.

II. Experimental Details

The SERS active silver colloid was prepared by citrate reduction of AgNO₃.²⁷ AgNO₃ (90 mg) was dissolved in 650 mL of quartz distilled water. Five hundred milliliters of this solution was brought to boiling and then a solution of 1% sodium citrate (10 mL) was added. Thirty minutes later the remaining 150 mL AgNO₃ solution was added 3 times every 15 min. The solution was kept on boiling about 1.5 h. The final Ag nanoparticle concentration was estimated to be ≈ 35 pM with an average radius size of about 40 nm.²⁸

PATP ethanol solutions of different concentration were mixed with the Ag sol solution in the same volume, respectively, and the measurement was performed immediately after the addition of the PATP. Time-dependent extinction spectra were measured (see Figure 2a–c) with absorption spectroscopy (Hitachi U3010). The structural evolution of the AgNP aggregates after the addition of PATP was measured after 3 days using dynamic light scattering (Dyn a Pro Nanostar, Mode No: WDPN-01, Wyatt Technology Corporation).

(25) Turansky, R.; Konpka, M.; Doltsinis, N. L.; Stich, I.; Marx, D. *ChemPhysChem* **2010**, *11*, 345.

(26) Yoon, J. H.; Park, J. S.; Yoon, S. *Langmuir* **2009**, *25*, 12475.

(27) Lee, P. C.; Meisel, D. *J. Phys. Chem.* **1982**, *86*, 3391.

(28) Xu, H. X.; Kall, M. *ChemPhysChem* **2003**, *4*, 1001.

The solution of PATP in ethanol was introduced into capillary sample cells for normal Raman measurement. The solution of PATP in aqueous silver sol with different concentrations was introduced into capillary sample cells for SERS measurement. The time-dependent SERS spectra were recorded by a Renishaw inVia Raman system equipped with an integral microscope (LEICA, DMLM). A 514.5 nm 25 mW air-cooled argon ion laser (Laser Physics, Model 25s-514) and a 632.8 nm 25 mW air-cooled argon ion laser (Laser Physics, Model 25s-514) were used as excitation sources. In our Raman experiment, the laser power used on the SERS sample was limited to 2 mW with 50 \times objective. The appropriate holographic notch filter was set in the spectroscopy. The holographic grating (1800 grooves/mm) and the slit allowed for a spectra resolution of 1 cm^{-1} . The spectrometer was measured to be $\leq \pm 0.2 \text{ cm}^{-1}$. Raman scattering was detected using a Peltier-cooled CCD detector (576 \times 384 pixels). The data acquisition time used in the experiment was 10 s. The SERS spectrum excited at 1064 nm was obtained with a RFS 100/S FT-Raman Spectrometer (BRUKER).

III. Theoretical Methods

All of the quantum chemical calculations were done with the Gaussian 09 suite.²⁹ The Ag₅-DMAB-Ag₅ junction model (see Figure 1c) was employed to study the electronic structures and SERS spectra. The ground-state geometry of Ag₅-DMAB-Ag₅ junction was optimized using density functional theory (DFT),³⁰ PW91PW91 functional,³¹ 6-31G(D) basis set for C, N, S, and H and LANL2DZ basis set³² for Ag. With the optimized ground-state geometry, the SERS spectrum of Ag₅-DMAB-Ag₅ junction was simulated with the same functional and basis set at zero frequency and 632.8 nm, respectively. Other theoretical²⁴ and experimental³³ studies performed previously have revealed that PW91PW91 can best simulate the Raman spectra for such a molecule. With the optimized ground state geometry, optical absorption spectra of the Ag₅-DMAB-Ag₅ junction was calculated using the time-dependent DFT (TD-DFT) method³⁴ with the same functional and basis set. For comparison, the SERS and electronic transitions of PATP-Ag₅ complex (Figure 1d) were also simulated at the optimized ground-state geometry at the same theoretical level. To assign vibrational modes of DMAB with symmetry, their Raman spectra were calculated using the DFT method, PW91PW91 functional, 6-31G(D) basis set, at their optimized ground-state geometries at same theoretical level. Electronic structure and optical properties of isolated DMAB were also calculated, using the TD-DFT method and same functional and basis set. The orientation of charge transfer in electronic transitions was visualized using charge difference density.¹¹

The response of the electromagnetic enhancement factors to different wavelength in junctions of AgNPs and the distribution of the local electromagnetic field enhancement at 632.8 nm were

calculated using the finite-difference time-domain (FDTD) method,³⁵ which implemented in the FDTD solutions software.³⁶ The amplitude of the incident plane wave was set to be 1 V/m in the calculation, and the enhancement factors were by dividing the field intensity in the junctions to the incident field intensity.

IV. Results and Discussion

A. Evidence of DMAB Produced from PATP. For reasons of comparison, we measured the normal Raman scattering (NRS) spectrum of PATP powder, which can be seen in Figure 3a. The calculated NRS of PATP shows that the vibrational modes at 1084.5 and 1589.6 cm^{-1} are the $\nu_{\text{cc}} + \nu_{\text{cs}}$ and ν_{cc} . To compare with the experimental SERS measurement of PATP adsorbed on silver sol, we calculated the SERS spectrum of the PATP-Ag₅ complex, which can be seen in Figure 3b. Comparing Figure 3a,b, one can see that the profiles are similar. The vibrational mode at 1616 cm^{-1} in Figure 3b is the NH₂ scissor vibration.

We measured the SERS spectrum of the PATP solution in aqueous silver (the concentration of PATP is 5×10^{-6} M), which can be seen in Figure 3c,d. The profiles of Figure 3c,d are similar, but they are significantly different from that of Figure 3b, especially in the range 1100 to 1500 cm^{-1} . There are three strong Raman peaks at 1143, 1390, and 1432 cm^{-1} in Figure 3c,d. We simulated the SERS spectrum of PATP, using the model of the PATP-Ag₅ complex (see Figure 3b). It was found that the three strong Raman peaks were not present in the simulated SERS spectrum of PATP. In previous studies, these three strong peaks in Figure 3c,d were assigned as an irreducible representation of the b₂ symmetry in the benzenoid structure of adsorbed PATP on silver electrodes.¹³ Fujishima and co-workers doubted that the Raman peaks might be attributed to some surface azobenzene species, but they did not discuss it in detail.³⁷

To correctly interpret the SERS spectra, we simulated the SERS spectrum of DMAB at zero frequency of laser, using the model the Ag₅-DMAB-Ag₅ junction (see Figure 3e). By comparing the experimental and theoretical results (see Figure 3f), one can see that the profiles are almost the same, which is direct spectral evidence for DMAB produced from PATP by a selective catalytic coupling reaction on silver nanoparticles.²⁴ To provide solid evidence that the dimer actually forms by a selective catalytic coupling reaction on silver nanoparticles, we assign the vibrational modes of PATP-Ag₅ and Ag₅-DMAB-Ag₅ with the symmetry of each modes in range from 1000 to 1700 cm^{-1} , which are listed in Figure 4. Since the dimer involves additional modes (including a point of inversion), all vibrational modes may be classified as g and u in symmetry. For each ring mode (a, b, c, d, f in Figure 4), there are two modes of the dimer, one g and the other u (in phase vs out-of-phase). For the case of strong coupling, these two modes should be split and well separated. In our case, one is strong, while the other is very weak, and they are near degeneracy, indicating that this is the result of weak coupling. It is found that all of ring vibrational modes of a, b, c, d, f are ring modes and their totally symmetric modes are strongly enhanced though the plasmon-only (electromagnetic field) enhancement. The vibrational mode at 1432 cm^{-1} is the N=N vibration. It is a symmetric vibration, which is also from a plasmon-only (electromagnetic field) enhancement. So, all six strong vibrational modes are all of g symmetry, enhanced by the electromagnetic field. Detailed

(29) Frisch, M. J.; Trucks, G. W.; Schlegel, H. B.; Scuseria, G. E.; Robb, M. A.; Cheeseman, J. R.; Scalmani, G.; Barone, V.; Mennucci, B.; Petersson, G. A.; Nakatsuji, H.; Caricato, M.; Li, X.; Hratchian, H. P.; Izmaylov, A. F.; Bloino, J.; Zheng, G.; Sonnenberg, J. L.; Hada, M.; Ehara, M.; Toyota, K.; Fukuda, R.; Hasegawa, J.; Ishida, M.; Nakajima, T.; Honda, Y.; Kitao, O.; Nakai, H.; Vreven, T.; Montgomery, J. A., Jr.; Peralta, J. E.; Ogliaro, F.; Bearpark, M.; Heyd, J. J.; Brothers, E.; Kudin, K. N.; Staroverov, V. N.; Kobayashi, R.; Normand, J.; Raghavachari, K.; Rendell, A.; Burant, J. C.; Iyengar, S. S.; Tomasi, J.; Cossi, M.; Rega, N.; Millam, J. M.; Klene, M.; Knox, J. E.; Cross, J. B.; Bakken, V.; Adamo, C.; Jaramillo, J.; Gomperts, R.; Stratmann, R. E.; Yazyev, O.; Austin, A. J.; Cammi, R.; Pomelli, C.; Ochterski, J. W.; Martin, R. L.; Morokuma, K.; Zakrzewski, V. G.; Voth, G. A.; Salvador, P.; Dannenberg, J. J.; Dapprich, S.; Daniels, A. D.; Farkas, O.; Foresman, J. B.; Ortiz, J. V.; Cioslowski, J.; Fox, D. J. *Gaussian 09*, Revision A.02; Gaussian, Inc.: Wallingford CT, 2009.

(30) Hohenberg, P.; Kohn, W. *Phys. Rev.* **1964**, *136*, B864–B867.

(31) Perdew, J. P.; Burke, K.; Wang, Y. *Phys. Rev. B* **1996**, *54*, 16533.

(32) Hay, P. J.; Wadt, W. R. *J. Chem. Phys.* **1985**, *82*, 270.

(33) Liu, Y. C.; McCreery, R. L. *Anal. Chem.* **1997**, *69*, 2091.

(34) Gross, E. K. U.; Kohn, W. *Phys. Rev. Lett.* **1985**, *55*, 2850.

(35) Kunz, K. S.; Luebber, R. J. *The Finite Difference Time Domain Method for Electromagnetics*; CRC: Cleveland, OH, 1993.

(36) *FDTD Solutions*, version 6.5; Lumerical Solutions, Inc., Vancouver, British Columbia, Canada, 2009.

(37) Yang, X. M.; Tryk, D. A.; Ajito, K.; Hashimoto, K.; Fujishima, A. *Langmuir* **1996**, *12*, 5525.

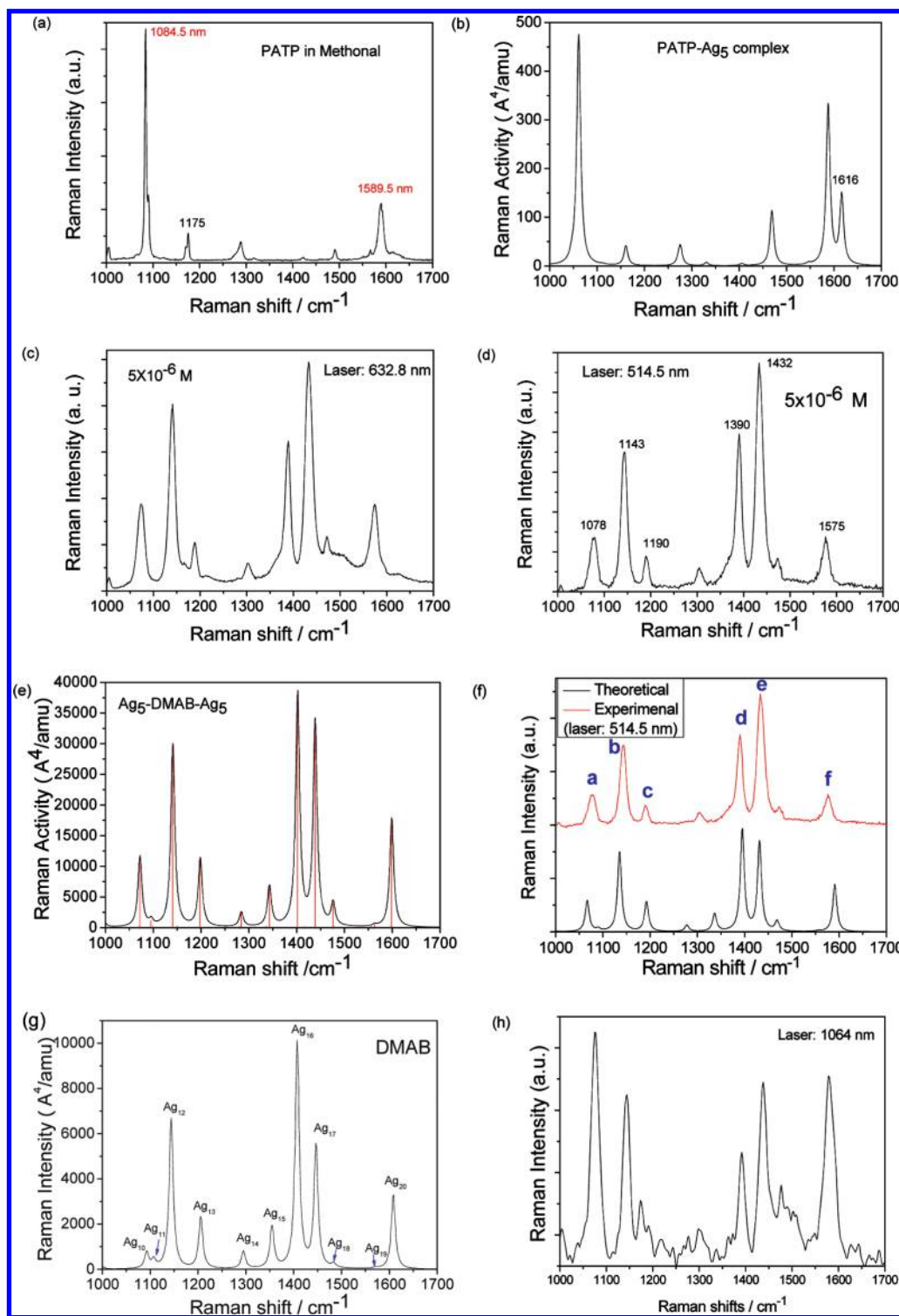


Figure 3. (a) The experimental normal Raman spectrum of PATP, (b) theoretical SERS spectrum of PATP-Ag₅ complex, (c) experimental SERS spectra of DMAB excited at 632.8 nm, (d) experimental SERS spectra of DMAB excited at 514.5 nm, (e) the calculated SERS spectrum of Ag₅-DMAB-Ag₅ junction, (f) comparisons between theoretical and experimental spectra, (g) the calculated Raman spectrum of isolated DMAB, and (h) the SERS spectrum excited at 1064 nm.

analysis of all vibrational modes of isolated DMAB with symmetry can be seen in Figure 3g and Table 2. There are four kinds of symmetries (A_g , B_u , A_u , B_g) for isolated DMAB. The vibrational modes of B_g and A_u symmetries are less than 1000 cm^{-1} , and the intensities are $0\text{ A}^4/\text{amu}$. The Raman peaks in Figure 3g are all arise from A_g symmetry, and the near degenerated B_u modes (intensities of $0\text{ A}^4/\text{amu}$) are listed in Table 2.

For the PATP, the Raman signals around 1143, 1390, and 1432 cm^{-1} are very weak (see Figure 3(a) and (b)), but they are significantly enhanced for DMAB (see Figure 3(c) and (d)), due to the formation of the $-N=N-$ bond of DMAB. These three strongly enhanced vibrational modes are direct evidence for the formation of DMAB from PATP via the $-N=N-$ bond. Using time-dependent SERS of DMAB, we will provide further

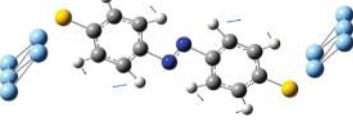
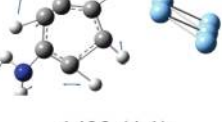
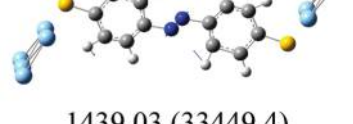
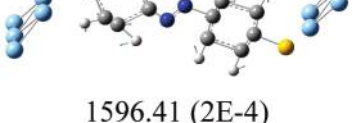
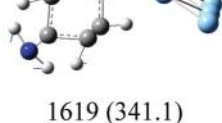
	DMAB	PATP
a	 1071.56 (0.0354)	 1082 (485.6)
b	 1141.31 (29874.5)	 1300 (41.0)
c	 1198.62 (11145.9)	 1183 (41.3)
d	 1402.44 (38019.1)	 1433 (4.1)
e	 1439.03 (33449.4)	
f	 1596.41 (2E-4)	 1619 (341.1)

Figure 4. Assignment of the vibrational modes of PATP-Ag₅ and Ag₅-DMAB-Ag₅, where vibrational frequencies (cm⁻¹) and Raman Activity (A⁴/amu) (in the parentheses) were also shown.

evidence for DMAB produced from PATP by selective catalytic coupling reaction on silver nanoparticles (see Section B).

B. Time-Dependent SERS of DMAB. We have observed the SERS of PATP adsorbed on noble metal surface strongly depend on the delay time and the concentration of PATP and silver sol. Figure 5a is time-dependent SERS spectrum of DMAB at the molecular concentration of 5×10^{-6} M. It is found that the SERS intensity increase gradually from 0 to 27 min, reaching a maximum at 27 min. After 27 min, the SERS intensity gradually decreases until after 50 min, a plateau is reached. From 0 to 27 min, Figure 5b demonstrates the rate of increase of SERS intensity of the $-N=N-$ relative vibrational modes at 1390 and 1432 cm⁻¹ and the C–N vibrational mode at 1143 cm⁻¹ is much larger than that of other modes, such as those at 1100 to 1500 cm⁻¹. This further supports the notion that DMAB is produced from PATP by a selective catalytic coupling reaction on silver nanoparticles. This dynamic process of SERS can be interpreted through three processes. The first process is the

adsorption of PATP molecules onto the silver nanoparticles through a thio group. The second process is the formation of DMAB, and the third is the aggregation of Ag nanoparticles linked by DMAB. In our experiment, these three processes coexist. From 0 to 27 min, the dominant process is the formation of DMAB produced from PATP on silver nanoparticles. Here, a few AgNPs were assembled to produce small AgNPs aggregates, which are capable of producing large electromagnetic field enhancements. From Figure 5b, we can see that the intense peaks at 1140, 1390, and 1432 cm⁻¹ representing the $-N=N-$ double bond formation increased more rapidly than other peaks. Note that the optical forces could also act some roles that drive more molecules to the “hot site” and make the nanoparticles closer to obtain higher EM enhancement.^{38,39} From 27 to 50 min, the size increase of the aggregated AgNPs linked by DMAB is the dominant process. These particles are too large for SERS experiments and,

(38) Xu, H. X.; Käll, M. *Phys. Rev. Lett.* **2002**, *89*, 246802.

(39) Svedberg, F.; Li, Z. P.; Xu, H. X.; Kall, M. *Nano Lett.* **2006**, *6*, 2639.

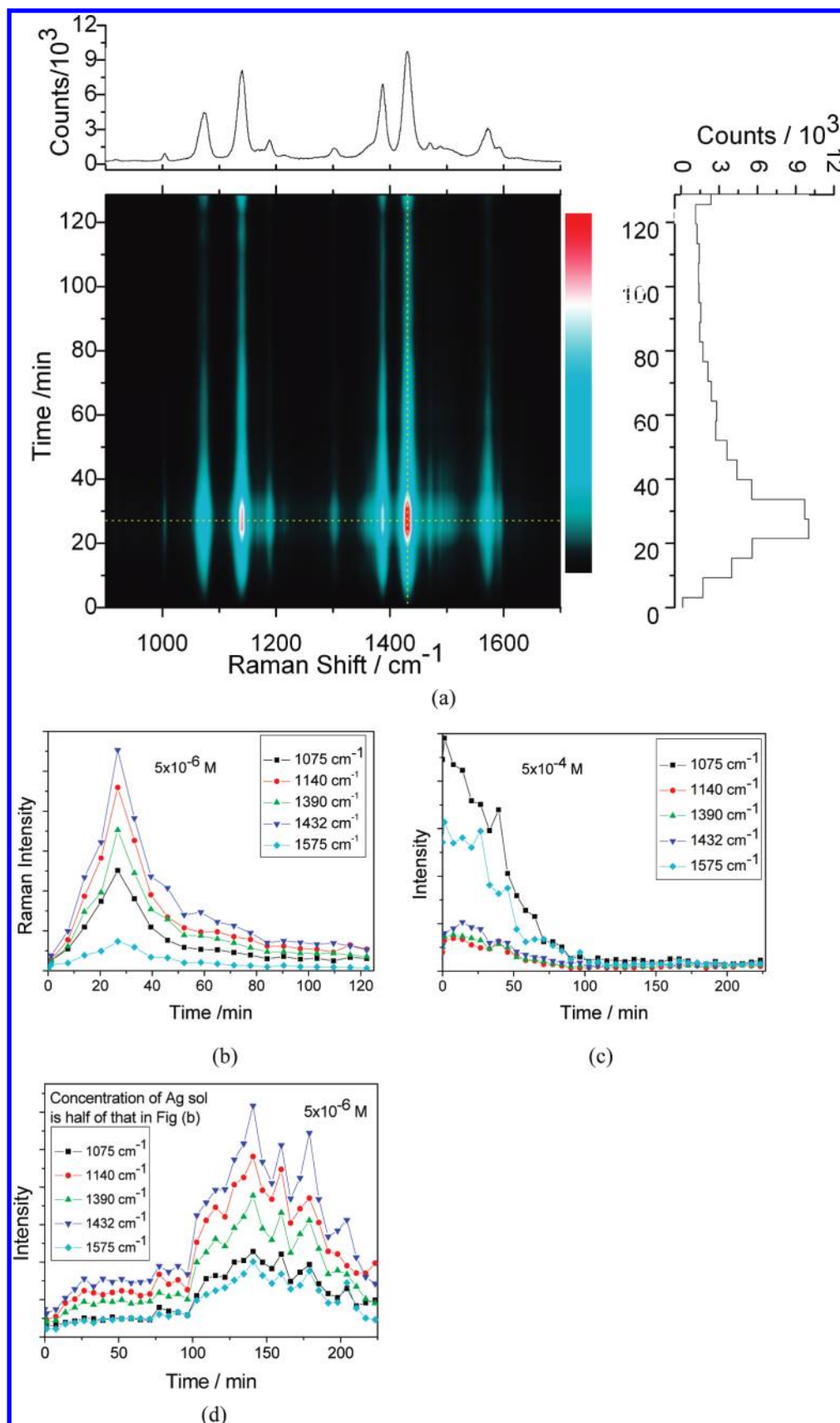


Figure 5. (a) The time-dependent SERS of DMAB at molecular concentration of M , (b) the time-dependent SERS intensities of DMAB for five vibrational modes with different acquired sequence (different time) at molecular concentration of M , (c) the time dependent SERS intensities of DMAB for five vibrational modes at the concentration of M , and (d) time dependent SERS intensities of DMAB for five different vibrational modes at the concentration of M , but the concentration of Ag sol is half of that in Figure 5(b).

Table 1. AgNP Aggregate at Different Concentration of PATP Measured Using Dynamic Light Scattering after 3 Days Later

concentration (M)	radius (nm)	S %
5×10^{-6}	76.7	2.60%
5×10^{-5}	229	6.50%
5×10^{-4}	351	7.10%
5×10^{-3}	441	8.90%

Table 2. Vibrational Modes of DMAB with Symmetry in Region from 1000 to 1650 cm^{-1} and Raman Activity (A^4/amu) (in the Parentheses)

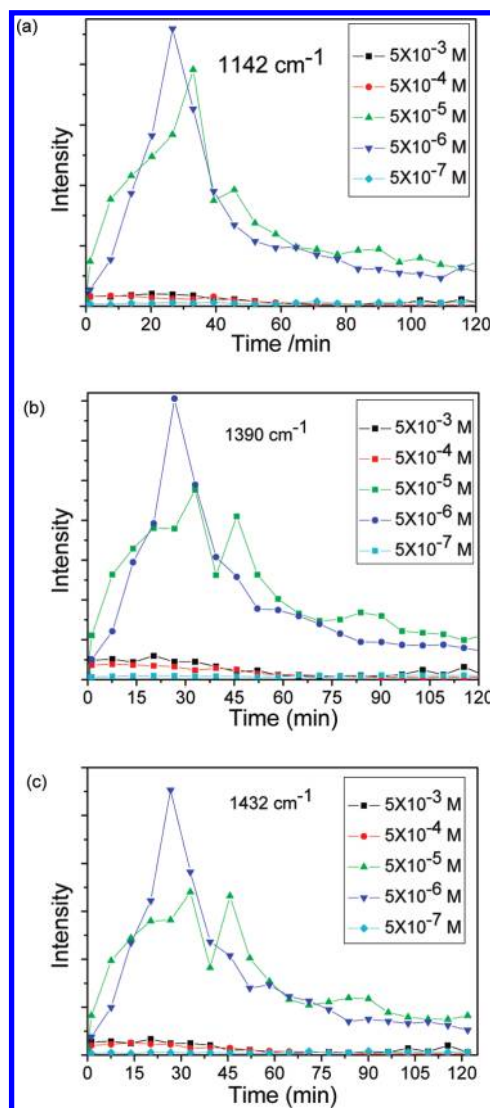
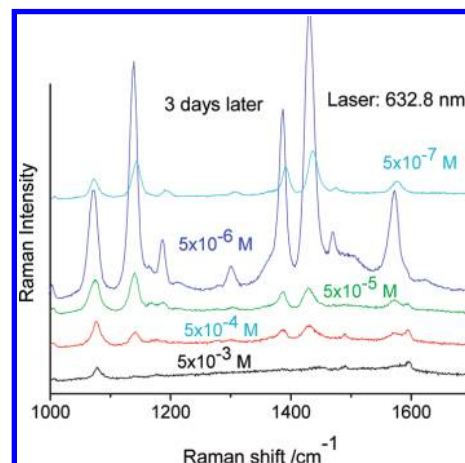
Bu ₁₀ : 1090.9 (0)	Ag ₁₀ : 1091.7 (721.0)
Ag ₁₁ : 1106.3 (359.9)	Bu ₁₁ : 1109.4(0)
Ag ₁₂ : 1143.2 (6656.6)	Bu ₁₂ : 1153.6 (0)
Ag ₁₃ : 1205.1 (2291.5)	Bu ₁₃ : 1255.9 (0)
Bu ₁₄ : 1290.5 (0)	Ag ₁₄ : 1294.4 (777.0)
Bu ₁₅ : 1350.0 (0)	Ag ₁₅ : 1354.4 (1858.7)
Ag ₁₆ : 1407.2 (10098.9)	Bu ₁₆ : 1428.6 (0)
Ag ₁₇ : 1446.5 (5432.9)	Bu ₁₇ : 1485.4 (0)
Ag ₁₈ : 1483.6(173.6)	Ag ₁₉ : 1571.6 (46.4)
Bu ₁₈ : 1565.9 (0)	Ag ₂₀ : 1608.5 (3292.6)
Bu ₁₉ : 1606.1 (0)	

consequently, only particles on the surface of the aggregates are capable of sustaining SERS signals. After 50 min, the aggregated Ag nanoparticles remain stable in suspension. The structural evolution of the AgNP aggregates was measured using dynamic light scattering (DLS). The size of the aggregated Ag nanoparticles remaining stable in the suspension are listed Table 1.

To demonstrate the time-dependent aggregation of Ag nanoparticles, we have acquired the extinction spectra of the Ag nanoparticle sol with different concentration of PATP as a function of time as shown in Figure 2a,b. The spectrum represented by the black line shows the surface plasmon absorption of the dispersed Ag nanoparticles before aggregation occurs. After the addition of PATP, as time passes the intensity of the surface plasmon band at 442 nm decreases, and the absorption in the long-wavelength region broadens and red shifts. The new absorption band in the long-wavelength region is attributed to the dipole plasmon resonance excitation of the coupled nanoparticles. As the DMAB attaches to AgNPs, the dipole peak at 442 nm shifts further to red and the coupling peak at long-wavelength appears. After a period of time, the AgNPs aggregates became increased in size. Consequently, the dipole peak would decrease and if the aggregates were big enough, the peak would be disappeared completely. Figure 2c is the extinction spectra of PATP in Ag sol after 3 h. The evolution of the UV–visible extinction spectrum is consistent with the structural evolution measured by DLS.

When the concentration of the added PATP was 5×10^{-4} M, we found that the Raman intensity decreased from the beginning, and subsequently, the Raman signal changed from its strongest value to almost constant within 50 min (see Figure 5c). Conversely, the SERS intensities at 1390 and 1432 cm^{-1} ($-\text{N}=\text{N}-$ relative vibrational modes) are much smaller than those at 1084 and 1575 cm^{-1} , and nearly equal to the background noise. So, with the increase in PATP concentration, the rate at which the DMAB is produced from PATP decreases. When the 5×10^{-6} M concentration PATP molecule solution was added to the silver sol that is diluted to half of the concentration used in the former experiment, we were able to see that the Raman signal was most intense in the range of 100–200 min (see Figure 5d). This shows that the acquisition time of the DMAB to be produced from PATP in silver sol will be increased as the concentration of silver sol is decreased.

We also studied the molecular concentration dependent normal modes from the SERS response of DMAB. From Figure 6, we can see that with a 35 pM concentration of the Ag sol the

**Figure 6.** Time dependent SERS intensities at (a) 1142, (b) 1390, and (c) 1432 cm^{-1} in different concentrations.**Figure 7.** The SERS of DMAB measured 3 day later at different concentrations of PATP at the incident light of 632.8 nm.

Raman signals at intensities at 1143, 1390, and 1432 cm^{-1} are strongest at the delay time of 27 min, when the concentration of PATP is 5×10^{-6} M. More experimental data show that a slightly

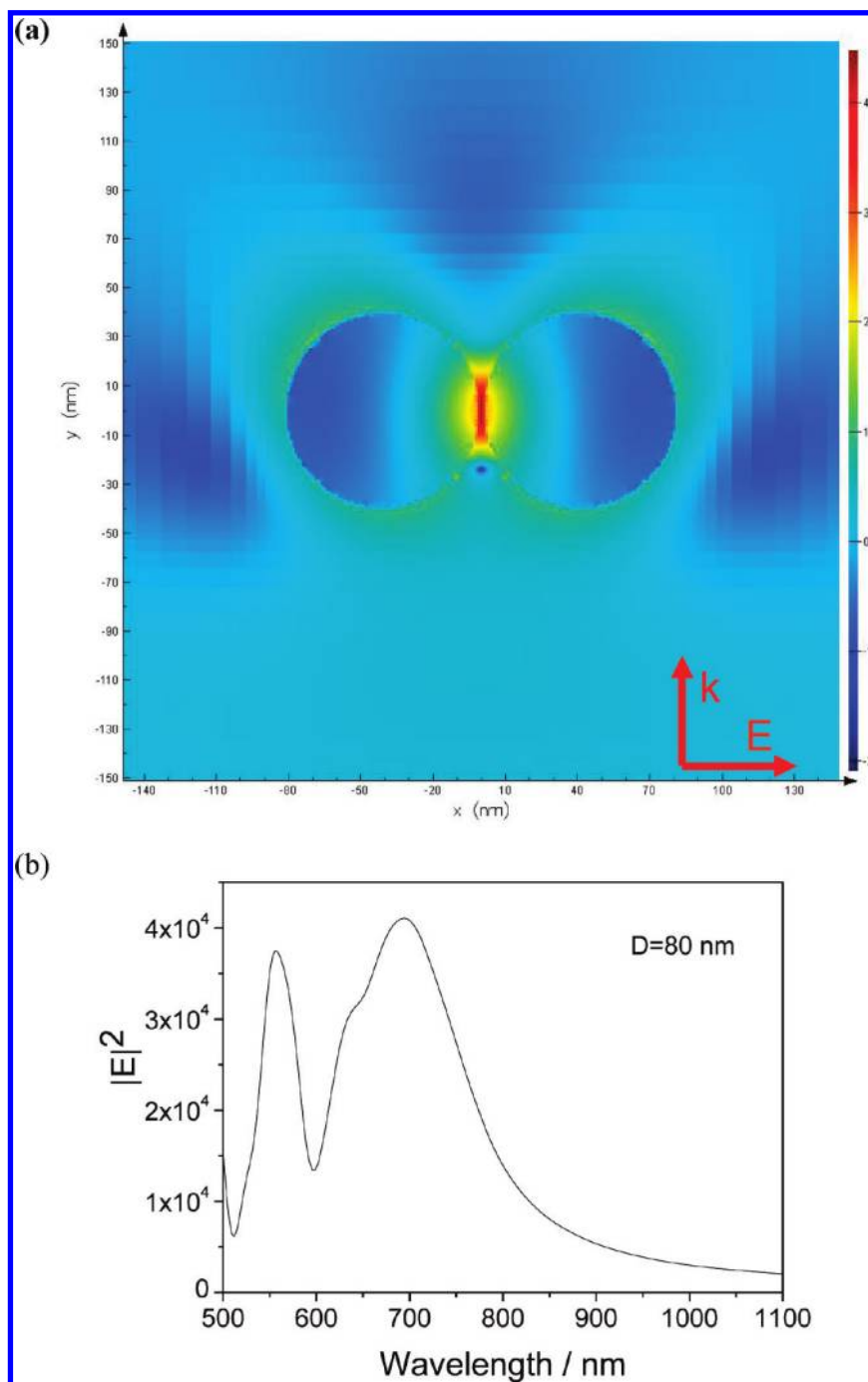


Figure 8. (a) The distribution of the local electromagnetic field enhancement at 632.8 nm in junctions of AgNPs. (b) The response of the electromagnetic field enhancement factors to different wavelength.

higher concentration of PATP will make the signal stronger (data not show). Thus we can be able to estimate that the best ratio of the AgNPs to the PATP molecules is about $7:10^6$. Furthermore, if we adjust the ratio carefully, we can make it arrive at its strongest signal at a long-run time.

To study the stability of the molecular concentration dependent SERS of DMAB, we measured the SERS of DMAB three days later at 632.8 nm. From Figure 7, one can find that the best SERS spectrum of DMAB is still at 5×10^{-6} M, and $-N=N-$ relative vibrational modes at 1390 and 1432 cm^{-1} can still be clearly observed. Moreover, we also find that 150 W power ultrasonic treatment and exposure to temperatures as high as 100 C cannot break the $-N=N-$ bond.

C. Electromagnetic and Chemical Enhancement Mechanisms.

The responses of the enhancement factors to different wavelengths of illumination in junction of AgNPs were calculated using FDTD solutions. The FDTD results reveal the distribution of the strongest local electromagnetic field enhancement is in junctions of AgNPs (see Figure 8a). The enhancement factors response to different wavelength at junctions can be seen from Figure 8b. It is found that the strongest local electromagnetic field enhancement is $(|M|^2 = |E_{\text{local}}|^2/|E_0|^2) 3 \times 10^4$ in the junctions of AgNPs, where the E_{local} and E_0 are the local and incident electric fields, respectively. The strongest SERS enhancement $(|M|^4)$ in junctions of AgNPs at 632.8 nm is 9×10^8 .

There are two kinds of chemical enhancement mechanisms. One is the static chemical enhancement via charge transfer between molecule and surface at the ground state (0.085 e is transferred from clusters to molecule), which results in the increase of static polarizability (see Table 3) and subsequently the increase of the SERS intensity of DMAB. By comparing the Raman intensities in Figure 3e,g, the ratios of the static chemical enhancement for six strongly enhanced modes are less than 20 (see Table 4). The second is the resonance enhancement via charge transfer in resonant electronic transition. To demonstrate this, electronic transitions in optical absorption of Ag₅-DMAB-Ag₅ complex were calculated (see Table 5). It is found that the SERS of DMAB is resonant Raman scattering, while the oscillator strength near 632.8 nm is very small.

The orientation of charge transfer for electronic transitions near 632.8 nm was visualized with charge difference density (see Figure 9). It is found that S₈ is an intermolecular charge transfer excited state, where electrons transfer from molecule to two Ag₅ clusters, while S₁₂ and S₁₆ are intramolecular charge transfer excited states. We calculated the SERS spectrum of DMAB using incident light of 632.8 nm. Here, the Raman activity at 1078 cm⁻¹ was known to be 4.6 × 10⁵ A⁴/amu. By comparing this with the Raman activity (721 A⁴/amu) of isolated DMAB for the same vibrational mode, we can see that the resonance Raman enhancement is 6.2 × 10² times. It is found that the resonance effect on the SER enhancement is not very strong, since the oscillator strengths on electronic transitions near 632.8 nm are very small. The enhancement factor of the resonance effect is proportional to the

Table 3. Calculated Static Electronic Polarizability Components in au^a

	<i>xx</i>	<i>yy</i>	<i>zz</i>
Ag ₅ -DMAB-Ag ₅	1249	637	459
DMAB	537	163	64
PATP	135	84	39

^aThe Cartesian coordinate can be seen from Figure 1.

Table 4. The Ratio of I_{SERS}/I_{DMAB} by Static Chemical Enhancement

vibrational modes	I _{SERS} (A ⁴ /amu)	I _{DMAB} (A ⁴ /amu)	I _{SERS} /I _{DMAB}
a	11561	721	16.0
b	29875	6656	4.5
c	11146	2291	4.9
d	38019	10098.9	3.8
e	33449	5432.9	6.2
f	17773	1608.5	16.6

Table 5. Singlet–Singlet Electronic Transitions of Ag₅-DMAB-Ag₅ Junction, DMAB, and PATP, Where *f* is Oscillator Strength (values shown in bold are of large oscillator strengths (*f*) in optical absorption)

	Ag ₅ -DMAB-Ag ₅	DMAB	PATP ^a	PATP ^b
S ₁	685.62 nm, <i>f</i> = 0.0000	¹ B _g , 560.29 nm, <i>f</i> = 0.0000	¹ A', 312.31 nm, <i>f</i> = 0.0300	300 nm
S ₂	685.61 nm, <i>f</i> = 0.0000	¹ B _u , 448.40 nm, <i>f</i> = 1.1945	¹ A'', 306.62 nm, <i>f</i> = 0.0000	
S ₃	641.86 nm, <i>f</i> = 0.0000		² A', 246.59 nm, <i>f</i> = 0.3345	250 nm
S ₄	641.85 nm, <i>f</i> = 0.0000		³ A', 231.91 nm, <i>f</i> = 0.0027	
S ₅	641.82 nm, <i>f</i> = 0.0001		² A'', 230.50 nm, <i>f</i> = 0.0000	
S ₆	641.79 nm, <i>f</i> = 0.0000		³ A'', 216.92 nm, <i>f</i> = 0.0000	
S ₇	600.95 nm, <i>f</i> = 0.0000		⁴ A'', 214.52 nm, <i>f</i> = 0.0003	
S ₈	600.91 nm, <i>f</i> = 0.0045		⁵ A'', 213.76 nm, <i>f</i> = 0.0000	
S ₉	598.10 nm, <i>f</i> = 0.0000		⁴ A', 201.93 nm, <i>f</i> = 0.0088	
S ₁₀	532.09 nm, <i>f</i> = 0.0000		⁵ A', 192.11 nm, <i>f</i> = 0.0754	
S ₁₁	532.09 nm, <i>f</i> = 0.0001		⁶ A'', 189.77 nm, <i>f</i> = 0.0000	
S ₁₂	531.24 nm, <i>f</i> = 0.9002		⁷ A'', 184.14 nm, <i>f</i> = 0.0000	
S ₁₃	510.58 nm, <i>f</i> = 0.0000		⁶ A', 183.83 nm, <i>f</i> = 0.5078	200 nm
S ₁₄	504.85 nm, <i>f</i> = 0.0006			
S ₁₅	504.85 nm, <i>f</i> = 0.0000			
S ₁₆	493.68 nm, <i>f</i> = 0.4122			

^aCalculated results with TD-PW91PW91/6-31G(D)//DFT-PW91PW91/6-31G(D). ^bExperimental results taken from ref 13.

oscillator strength on electronic transitions. The strongest resonance SERS enhancement on the order of 10⁵ was reported theoretically.⁴⁰ Thus, the total chemical enhancements reported in this paper, including static chemical enhancement (less than 20 times) and resonant enhancements (6.2 × 10² times), are on the order of 10³.

We also calculated the electronic transitions of isolated DMAB. The group symmetry of DMAB is C_{2H}. We calculated electronic transitions with symmetry for first two lowest singlet states (see Table 5) and the orientation of charge transfer for these two excited states (see Figure 10). It was found that S₁ is dark state (¹B_g), which arises from the ¹⁶a_g→⁵b_g orbital transition and electron transfers from N=N bond to two outer sides. S₂, however, shows strong absorption (¹B_u), and arises from the ⁵a_u→⁵b_g orbital transition, and electron transfers from two sides to N=N bond. To confirm the reliability of the TD-PWP1PW91/6-31G(D) for electronic transitions of DMAB, electronic transitions of PATP with symmetry were calculated at the same theoretical level and compared with experimental Data in ref 13 (see Table 5). The group symmetry of PATP is C_{2V}. It is found that TD-PWP1PW91/6-31G(D)//DFT-PWP1PW91/6-31G(D) can reproduce the experimental optical absorption of PATP very well. Thus, it is reliable to predict electronic transitions of DMAB. The orientation of charge transfer for these three strong absorption peaks of PATP was visualized using charge difference density (see Figure 11).

D. DMAB Produced from PATP on Ag Substrates Excited at 1064 nm. The SERS spectrum in Figure 3h reveals that DMAB is produced from PATP on Ag substrates excited at 1064 nm through the presence of three Raman peaks at 1141, 1392, and 1440 cm⁻¹. Note that signal/noise ratio is low, since the electromagnetic field enhancement at 1064 nm is weak, where the diameter of AgNPs is 80 nm in our experiment, and the |M|² = 2.3 × 10³ (see Figure 8b).

SERS of PATP adsorbed on different substrates excited at 1064 nm, Zhou and co-worker have observed these three strong Raman peaks with PATP adsorbed on a Ag film (see Figures 3 and 5 in ref 41), on Ag nanoparticles (see Figures 2 and 4 in ref 20), and in the Ag/PATP/Ag assembly (see Figure 3 in ref 42). In fact, our simulation of the SERS spectrum at the Ag₅-DMAB-Ag₅ junction in Figure 4e sufficiently reproduces the experimental results in Figure 3 in ref 42. So, the evidence of DMAB produced from PATP on Ag substrates excited at 1064 nm has been provided by the SERS spectrum in Figure 3h.

For the Ag/PATP/Ag assembly, we simulated the enhancement factors response of different wavelength at the junctions of AgNPs using FDTD solutions. It was found that when the diameter of

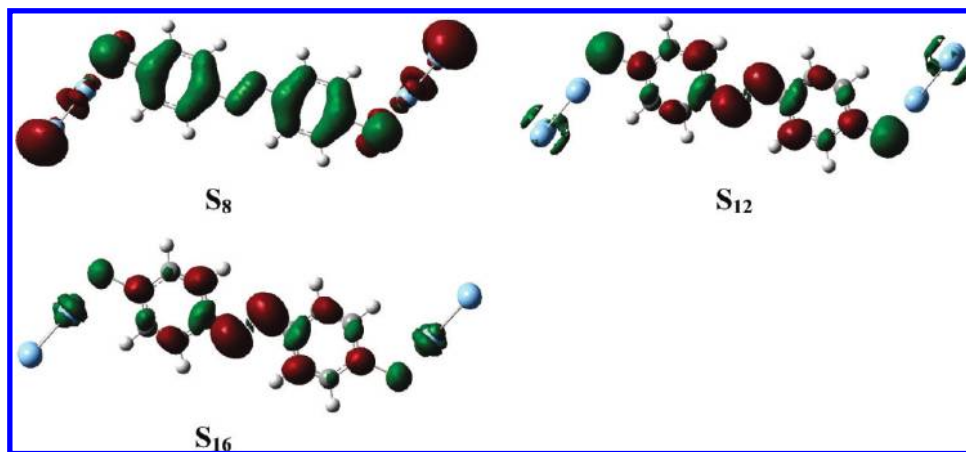


Figure 9. Charge difference densities for electronic transitions of $\text{Ag}_5\text{-DMAB-Ag}_5$, where green and red stand for hole and electron, respectively.

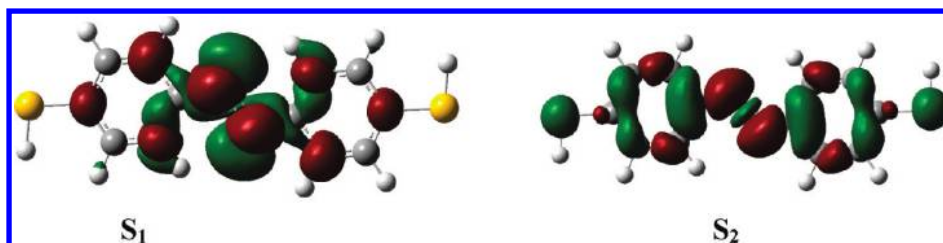


Figure 10. Charge difference densities for electronic transitions of DMAB, where green and red stand for hole and electron, respectively.

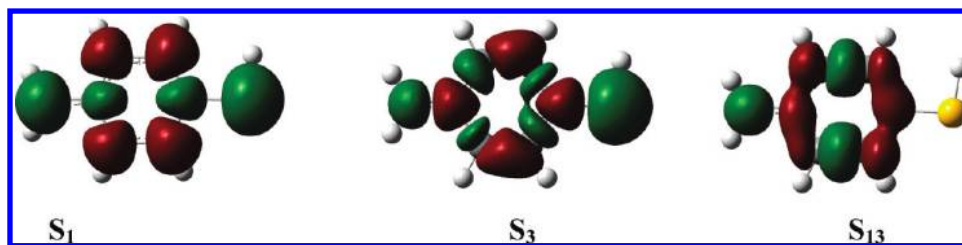


Figure 11. Charge difference densities for electronic transitions of PATP, where green and red stand for hole and electron, respectively.

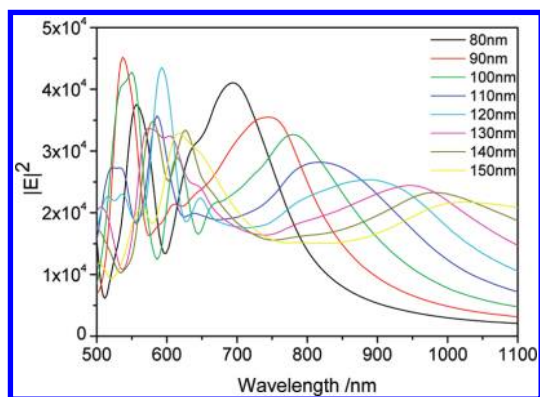


Figure 12. The response of the electromagnetic enhancement factors to different wavelength for different size AgNPs (dimer).

AgNPs is 150 nm, the strongest electromagnetic field enhancement is obtained (see Figure 12). Thus, 150 nm is the best AgNP size to observe the three Raman peaks of DMAB at 1142, 1390, and 1432 cm^{-1} . The strongest SERS enhancement is $|M|^4 = 4.0 \times 10^8$.

V. Conclusion

Direct experimental and theoretical evidence from SERS has been provided showing that DMAB is produced from PATP by selective catalytic coupling reaction on silver nanoparticles. It is found that the vibrational modes at 1390 and 1432 cm^{-1} are the ν_{NN} as well as symmetric ν_{CC} vibrations. By analyzing the symmetry of strongly enhanced vibrational modes, we deduce that all six strong vibrational modes are enhanced by plasmon (electromagnetic field). This is direct evidence for the formation of DMAB from PATP via the $-\text{N}=\text{N}-$ bond. The SERS intensity varies with the delay time and concentration of the Ag sol and the concentration of DMAB. To observe the SERS of DMAB in the concentration of 35 pM in Ag sol, the better experimental conditions are (1) the concentration of PATP is 5×10^{-6} M, and (2) the acquisition time is at 27 min for SERS measurement. The SERS enhancement ($|M|^4$) is on the order of $|M|^4 = 9.0 \times 10^8$ when illuminated the incident light of wavelength 632.8 nm. The total chemical enhancements, including static chemical and resonant enhancements, are on the order of 10^3 .

Acknowledgment. This work was supported by the National Natural Science Foundation of China (Grants 10874234, 20703064, 90923003), the National Basic Research Project of China (Grant 2009CB930701).

(40) Zhao, L. L.; Jensen, L. J.; Schatz, G. C. *Nano Lett.* **2006**, *6*, 1229.
 (41) Zhou, Q.; Zhao, H.; Pang, F.; Jing, Q.; Wu, Y.; Zheng, J. *J. Phys. Chem. C* **2007**, *111*, 514.
 (42) Zhou, Q.; Fan, Q.; Zhuang, Y.; Li, Y.; Zhao, G.; Zheng, J. *J. Phys. Chem. B* **2006**, *110*, 12029.